Magnetic structure and transport properties of noncollinear $LaMn_2X_2$ (X=Ge,Si) systems

S. Di Napoli[1] and A. M. Llois[1,2,*]
[1]*Departamento de Física, Facultad de Ciencias Exactas y Naturales, Universidad de Buenos Aires, 1428 Buenos Aires, Argentina*
[2]*Departamento de Física, Comisión Nacional de Energía Atómica, Avenida del Libertador 8250, 1429 Buenos Aires, Argentina*

G. Bihlmayer and S. Blügel
Institut für Festkörperforschung, Forschungszentrum Jülich, D-52425 Jülich, Germany

M. Alouani and H. Dreyssé
IPCMS-GEMME, UMR 7504 CNRS-ULP, 23 rue du Loess, F-67034 Strasbourg Cedex, France
(Received 4 May 2004; published 15 November 2004)

Electronic, magnetic, and transport properties of the noncollinear naturally multilayered compounds $LaMn_2Ge_2$ and $LaMn_2Si_2$ are addressed by first-principles calculations based on the density-functional theory. At low temperatures, these systems show a magnetic state with the Mn moments ordered in a conical arrangement (spin spiral) with a ferromagnetic coupling along the c axis and an in-plane antiferromagnetic coupling. The magnetic structures are studied by means of the full-potential linearized augmented-plane-wave method within both the generalized-gradient approximation and the local-density approximation. In both compounds, a conical magnetic state is obtained with energies lower than canted and collinear structures. The trends in the experimentally observed magnetic configuration when replacing Ge by Si are discussed. The origin of the experimentally observed inverse giant magnetoresistance in $LaMn_2Ge_2$ is traced back to the presence of many noncollinear low-energy magnetic configurations.

DOI: 10.1103/PhysRevB.70.174418 PACS number(s): 72.25.Ba, 75.30.Ds, 75.47.De, 72.15.−v

I. INTRODUCTION

Noncollinear magnetism has been known for more than 40 years, and even though in recent years much progress has been achieved in the description of itinerant magnetic ordering, only few first-principles calculations have been performed for complex systems with a noncollinear magnetic ground state.[1–5] In the past decade, electronic structure methods have been extended to describe noncollinear spin structures within density-functional theory and the formalism has been mainly used to study magnetic excitations and finite-temperature properties of ferromagnets such as Fe, Co, or Ni.[6] First-principles calculations extended to noncollinear magnetism have not only been used to investigate finite-temperature properties of magnetic materials through the determination of magnon spectra and Curie temperatures, but they have also been applied to frustrated antiferromagnets,[7] γ-Fe,[8] and, lately, to the spin spirals appearing in the Heusler alloys, Ni_2MnGa and Ni_2MnAl.[1]

The magnetism of systems containing Mn exhibit a rich variety of magnetic ground-state structures. This behavior has its origin in the well-known fact that the magnetic moment and the exchange interactions of Mn are highly sensitive to geometry and interatomic distances. Antiferromagnetic interactions between nearest-neighbor atoms compete with ferromagnetic interactions between more distant atoms. External parameters determining the geometry can cause dramatic changes in the spin arrangement. For instance, bulk manganese itself crystallizes in complex structures such as the α and β phases with noncollinear spin arrangements.[3,4] The large magnetic moment of Mn gives a lot of weight to higher-order exchange interactions. For example, as a consequence monolayers of Mn deposited on Cu(111) display a noncollinear three-dimensional magnetic arrangement,[7] and families of compounds which have Mn as a constituent show frequently a rich variety of complex magnetic configurations depending on the Mn-Mn distances. Among these systems are the intermetallic ternary compounds of the type RMn_2X_2 (R=Ca, La, Ba, Y, etc., and X=Si, Ge) which crystallize in the $ThCr_2Si_2$ structure. The Mn-Mn distances in these structures are mainly determined by the size of the other atoms building the compound. For example, the in-plane lattice constant of $LaMn_2Ge_2$ and $LaMn_2Si_2$ is 4.19 Å and 4.11 Å, respectively. Experimentally they show a large variety of magnetic ground states which depend on R and X. The spins on the Mn sublattice can arrange in spiral spin-density waves (SSDW), antiferromagnetic (AFM), ferromagnetic (FM), or/and canted magnetic structures.[9–12] In these structures, the Mn atoms occupy every fourth layer stacked along the c axis. The Mn sublattice forms a simple tetragonal framework (cf. Fig. 1) and the Mn-Mn interlayer distance along the c axis, $R^c_{\text{Mn-Mn}}$, ranges between 5.4 and 5.6 Å, whereas the Mn-Mn intralayer distance, $R^a_{\text{Mn-Mn}}$, lies in the range of 2.8–3.2 Å, being roughly half the one corresponding to $R^c_{\text{Mn-Mn}}$.

Among the above-mentioned systems, the bulk magnetic properties of the compounds with R=La and X=Ge or Si show a complex magnetic structure which has been recently re-examined by neutron diffraction experiments.[12] At high temperatures, these systems are purely collinear antiferromagnets, showing a FM stacking of AFM (001) planes. At low temperatures, they present noncollinear magnetic structures with the magnetic moments of Mn ordered in a conical spin spiral along the c axis. The moments couple FM along the c axis, while they exhibit an AFM component within the (001) Mn planes. At a temperature of T=2 K, the wave vector $\mathbf{q}$ of the spin spiral of $LaMn_2Ge_2$ is oriented along the c

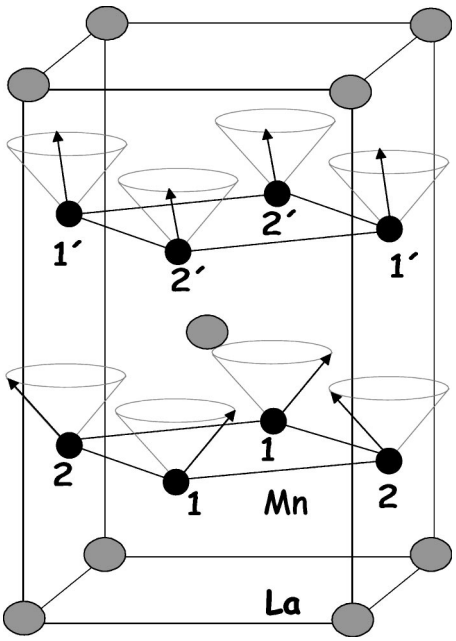

FIG. 1. Magnetic unit cell of $LaMn_2Ge_2$ at 2 K. The Ge atoms are not displayed. In the $ThCr_2Si_2$ (space group $I4/mmm$) structure, the rare-earth atoms occupy the (0,0,0) sites [Wyckoff position 2(a)] and the Ge atoms the $(0,0,\pm z)$ sites with $z \approx 0.38$ [Wyckoff position 4(e)]. The Mn atoms occupy the special position 4(d) at $(0,1/2,1/4)$ with an additional I translation mode (Ref. 12).

axis with an absolute value q_z of 0.71 $(2\pi/c)$, and the semicone or canting angle θ (measured from the c axis) is 58°, while for $LaMn_2Si_2$ the corresponding values are $q_z = 0.91$ $(2\pi/c)$ and $\theta = 25°$. The total Mn magnetic moments are $3.06\mu_B$ and $2.43\mu_B$ for $LaMn_2Ge_2$ and $LaMn_2Si_2$, respectively.[11,12]

The presence of conical helical magnetic order in $LaMn_2Ge_2$ and $LaMn_2Si_2$ makes these systems ideal candidates to study the evolution of the magnetic properties as a function of canting angle and helicity (q_z). To our knowledge, no *ab initio* calculations have been undertaken yet to study many-atom compounds exhibiting simultaneously conical and helical magnetic order. In this contribution, we investigate the magnetic and electronic structure of both compounds and show that, within the local-density approximation (LDA) to the density-functional theory (DFT), conical spin spirals are obtained as the ground states for both systems and that the values of the ground-state spin-spiral wave vectors $\mathbf{q}$ follow the experimental trends.

Another interesting feature of these systems is that for $X = Ge$, an inverse magnetoresistance has been reported.[13] In the past decade, characterized by the search of new materials with specific electronic and magnetic properties, much attention has been devoted to the transport properties of layered structures. In particular, the stress has been put on those showing a giant magnetoresistance[14] effect (GMR). The magnetoresistive properties are strongly dependent upon the magnetic structure, therefore its determination is crucial for the computation of the transport coefficients. We address in this work the dependence of the band contribution to GMR on the different magnetic configurations of $LaMn_2Ge_2$.

This paper is organized as follows. In Sec. II, the computational scheme and method of calculation are discussed. In Sec. III, the results of the calculations are presented and analyzed and Sec. IV is devoted to the concluding remarks.

II. METHOD OF CALCULATION

The calculations are performed self-consistently using the FLEUR code,[15] which is an implementation of the full-potential linearized augmented plane-wave (FLAPW) method[16] that allows the treatment of noncollinear magnetism including incommensurate spin spirals.[17] As there have been several discussions regarding the different exchange-correlation (XC) potentials to be used in the context of noncollinear magnetism, we present here the results obtained within the local-spin-density approximation (LSDA) to the XC potential and within the generalized-gradient approximation (GGA). The results obtained within both approximations are compared with the experimental ground-state configurations.

Although in noncollinear magnetic systems no global spin-quantization axis exists, at every point of space a local coordinate system can be defined such that the magnetization is locally oriented in the z direction. Since the LSDA depends only on the magnitude of the magnetization, the XC potential can be calculated at every point in the local coordinate system just as in the usual collinear case. The noncollinear potential is obtained by back-rotation to the global frame of reference. On the other hand, the GGA depends also on the gradients of the magnetization. As the direction of magnetization may vary, when calculating the gradients only projections of the magnetization on the local quantization axis are taken into account in the standard GGA implementations. If the magnetization direction varies slowly, this approximation is sufficient. Nonetheless, a previous study suggests that in some cases the disagreement between theory and experiment might come from the projection errors,[18] while in attempts to improve the GGA for noncollinear calculations the effects were found to be small.[19] We used the XC potential as given by Moruzzi, Janak, and Williams (MJW) (Ref. 20) in the case of the LDA calculations and by Perdew and Wang (PW) (Ref. 21) and Perdew, Burke, and Ernzerhof (PBE) (Ref. 22) for the GGA calculations.

The FLEUR code allows for the treatment of the noncollinear magnetism with magnetic moments M_α at an atomic site α oriented along arbitrarily chosen directions $\hat{\mathbf{e}}^\alpha$ as well as incommensurate spiral spin-density-wave (SSDW) states. Assuming a rotation of the spins around the z axis, the components of the local magnetic moments of an atom with the basis vector $\boldsymbol{\tau}^\alpha$ in the unit cell n (with the origin at the lattice vector $\mathbf{R}^n$) are given in the global reference frame by

$$\hat{\mathbf{e}}^{n\alpha} = \begin{pmatrix} \cos[\mathbf{q}\cdot(\mathbf{R}^n + \boldsymbol{\tau}^\alpha) + \xi^\alpha]\sin\,\theta^\alpha \\ \sin[\mathbf{q}\cdot(\mathbf{R}^n + \boldsymbol{\tau}^\alpha) + \xi^\alpha]\sin\,\theta^\alpha \\ \cos\,\theta^\alpha \end{pmatrix}. \quad (1)$$

For more than one magnetic atom in the unit cell, an additional atom-dependent phase, ξ^α, has been introduced in the above equation. As suggested by the experiment,[12] we

have chosen a phase shift $\Delta\xi=\pi$ for the two Mn atoms in the (001) plane for both $LaMn_2Ge_2$ and $LaMn_2Si_2$. The semicone angles θ have been found to be identical for the two atoms.

In the implementation of the FLEUR code, the magnetization is treated as a continuous vector field in the interstitial region, while inside each muffin-tin sphere an average direction of magnetization is used. The 3*d* transition metals in open structures are elements showing weak intra-atomic noncollinearity, and for Mn the magnetic moments are fairly large, therefore we believe that our implementation is most appropriate for the systems under study. The SSDWs are treated by means of the generalized Bloch theorem,[23] which states that, in the absence of the spin-orbit coupling, a generalized translation operator can be defined combining the regular translations in the Bravais lattice with the rotation in the spin space.[17] Due to the generalized Bloch theorem, even incommensurate spin spirals with the underlying lattice can be studied restricting the calculation to the chemical unit cell and thus no large supercells are needed. Since spin-orbit coupling is neglected, the directions in spin space and real space are not coupled and all calculated quantities depend only on the relative orientations of the magnetic moments.

In our calculations, the **k**-point set used corresponds to 100 **k** points in the irreducible wedge of the Brillouin zone (IBZ), which corresponds to 1/4 of the total unit cell in the case of a noncollinear configuration. The tetragonal magnetic unit cell contains ten atoms and the calculations are performed including all basis functions with wave vectors smaller than $K_{\max}=3.4$ a.u.$^{-1}$, leading to about 95 basis functions per atom. The convergence of the energies with respect to these quantities has been carefully checked. The number of **k** points and $K_{\max}$ were chosen in such a way to ensure convergence of total energy differences to 10^{-3} eV. The La 5*s* and 5*p* semicore states are treated as valence states and are described by local orbitals, which are added to the LAPW basis set. The muffin-tin radii have been set to 2.3 a.u. for all atoms.

To estimate the GMR ratio, i.e., the relative change in the resistivity as a function of an applied magnetic field, the conductivities are calculated within the semiclassical Boltzmann approach in the relaxation-time approximation.[24] As we are only treating the band contribution to the GMR ratio, the dependence of the relaxation time on **k** and spin is neglected, as well as the vertex corrections. In a first approximation, spin accumulation and interface disorder effects can be neglected because the present systems are natural multilayers with perfect interfaces. The semiclassical Boltzmann equation is valid only in the low impurity limit, and in the absence of vertex corrections the conductivity tensor is given by

$$\sigma^{ij}=\frac{e^2}{8\pi^2}\tau\sum_{\nu s}\int v^i_{\nu s}(\mathbf{k})v^j_{\nu s}(\mathbf{k})\,\delta(\epsilon_{\nu s}(\mathbf{k})-\epsilon_F)d^3k. \qquad (2)$$

The index *s* denotes spin, ν is the band index, ϵ_F is the Fermi energy, and τ is the relaxation time assumed to be independent of the scattering state and magnetic configuration. To compute the semiclassical velocities, $v^i_{\nu s}$, which are the derivatives of the energy with respect to k_i, $v^i_{\nu s}=1/\hbar\ \partial\epsilon_{\nu s}/\partial k_i$, we used 2475 **k** points in the IBZ. Equation (2) is computed by means of the tetrahedron method.[25] As a general expression for the giant magnetoresistance, we use the definition

$$\mathrm{GMR}_i=\frac{\sigma^{ii}(\mathrm{NF})}{\sigma^{ii}(\mathrm{FM})}-1, \quad -1<\mathrm{GMR}<+\infty. \qquad (3)$$

With NF we indicate a nonferromagnetic configuration as, for instance, the AFM case or the noncollinear arrangements of the magnetic moments of Mn in $LaMn_2Ge_2$. If $i=z$, i.e., if *i* is along the *c* axis of the unit cell, GMR_z corresponds to the current perpendicular to the plane (CPP) GMR; if *i* is parallel to the plane of the unit cell, $\mathrm{GMR}_{x,y}$ is called current in-plane (CIP) GMR. Direct or negative GMR is indicated by a negative value of GMR: otherwise an inverse GMR is observed. With the approximations listed above made to the relaxation time, τ cancels out from Eq. (3).

III. RESULTS AND DISCUSSION

A. GGA versus LDA for $LaMn_2Ge_2$

Since the computation of conical helical structures is time-consuming, we decided to do first a preliminary study of the influence of the exchange-correlation (XC) potential on the ground-state magnetic configuration. With that purpose in mind, we made a systematic investigation of $LaMn_2Ge_2$. As mentioned in the Introduction, the magnetic ground state suggested by experiments has a SSDW along the (001) axis with $q_z=0.71\ (2\pi/c)$ and a semicone angle of 58° at 2 K. In Fig. 1, the magnetic and atomic structure of the system is shown.

In a first step, we optimized the lattice parameter of $LaMn_2Ge_2$ within the GGA and the LDA by keeping the c/a ratio at the experimental value of 2.616 and the internal parameter of the Ge atoms at $z=0.38$. Thus, the internal coordinates of the different atoms of the system were kept at the experimental values. We studied the dependence of the total energy, corresponding to different magnetic configurations, as a function of the volume. We considered a collinear ferromagnetic alignment (FM) of Mn moments, a configuration with antiferromagnetic alignments simultaneously in-plane as well as between the planes (AFM1), and a conical helical one for which experimental values for the **q** vector of the SSDW and for the canting angle have been used. In Figs. 2 and 3, we show the total energy per unit cell with respect to the energy of the FM configuration at the experimental in-plane lattice parameter as well as the evolution of the local Mn magnetic moment, μ_{Mn}, as a function of the in-plane lattice parameter *a*. The magnetic moment of all other atoms in the compound is small compared to the Mn ones, and therefore the cell magnetic moment per Mn atom is in good approximation (to 98%) given by the local Mn moment itself.

Figure 2 shows the results obtained within the GGA, given by Perdew and Wang (PW).[21] We did further calculations using the Perdew, Burke, and Ernzerhof (PBE) (Ref. 22) XC potential, but the results obtained are similar to those depicted here. From Fig. 2, it is seen that within the GGA,

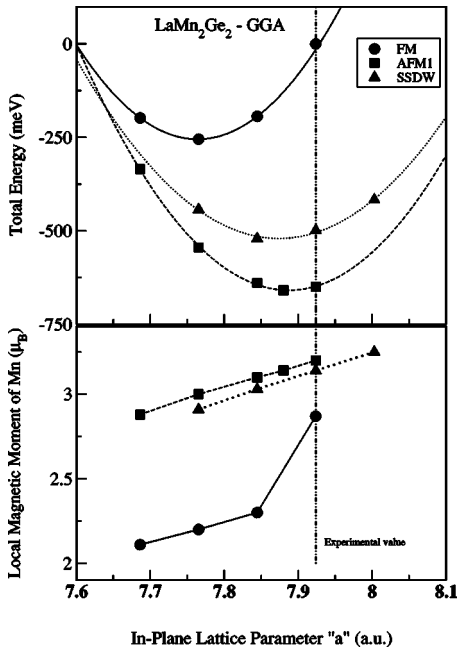

FIG. 2. Total energy per unit cell and local Mn magnetic moment of $LaMn_2Ge_2$ as a function of the in-plane lattice parameter a, calculated within the GGA. The c/a ratio was kept at the experimental value of 2.616 (Ref. 12). The vertical dashed-dotted line indicates the experimental equilibrium value a_0.

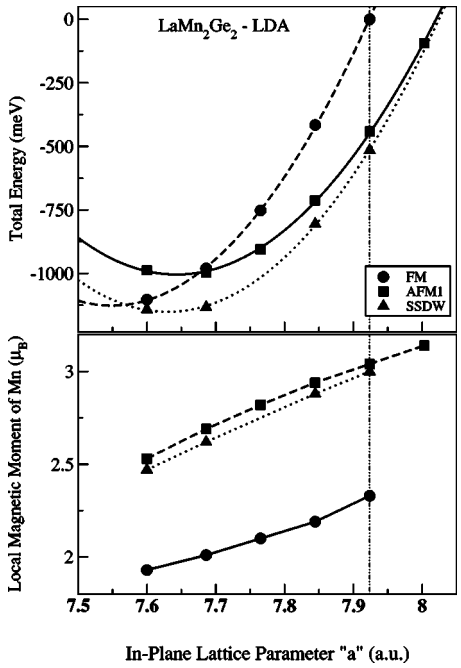

FIG. 3. Same as Fig. 2 but for the LDA.

the AFM1 magnetic structure has the lowest total energy. It can be seen that within the GGA, the optimized in-plane lattice parameter, for the AFM1 configuration, is less than 0.6% smaller than the experimental one. For this optimum in-plane lattice parameter, we have also optimized the internal coordinates of Ge by force calculations. We found that the Ge-Mn distance is 1.3% smaller than the experimental value. At the minimum total energy, the internal Ge coordinates are not significantly different from the experimental values; we decided to continue the analysis by keeping the latter values fixed. The magnetic moment per Mn atom at the optimized volume is $3.14\mu_B$, i.e., close to the corresponding experimental value. However, within the GGA, AFM1 is the magnetic ground structure, in disagreement with experiment.

The results obtained within the LDA are shown in Fig. 3. They display that the optimized in-plane lattice parameter, a_0, is 4% smaller than the experimental value. Also the magnetic moment per Mn atom at the optimized volume, $2.47\mu_B$, is much smaller than the value observed experimentally. But within the LDA, the SSDW is the magnetic structure with the minimum energy. The energy differences between the different magnetic structures are larger than the computational error bars. For the SSDW at the optimized lattice constant in the LDA, the total Mn moment is 19% smaller than the experimental value of $3.06\mu_B$, while it is in good agreement ($3.00\mu_B$) at the experimental volume. With decreasing volume a crossover to a FM ground state is observed, which is reasonable since the direct Mn-Mn exchange interaction for small interatomic distances is ferromagnetic.[26] The values of the magnetic moments of Mn depend strongly on the in-plane lattice parameter or, in other words, on the Mn-Mn distance, as pointed out in the Introduction, and this can be observed in Figs. 2 and 3.

Within the LDA, the SSDW configurations are those with the lowest energies, giving the proper experimental trends, while this is not the case within the GGA, for which the AFM1 structure is the one giving the lowest energy as a function of the in-plane lattice parameter. This is in line with the general observation that the GGA tends to increase the lattice parameters and magnetic moments, but as compared to the LDA (Ref. 27) it does not necessarily improve the description of magnetic materials. From this analysis, we decided to perform further calculations within the local-density approximation and use the experimental lattice parameters, both for $LaMn_2Ge_2$ and $LaMn_2Si_2$, in order to obtain magnetic moments close to the corresponding experimental values. The obtained results, both within the GGA and the LDA, are summarized together with the experimental values in Table I.

B. Magnetic properties at experimental volume within the LDA

1. Canted structures in $LaMn_2Ge_2$ *and* $LaMn_2Si_2$

For $\mathbf{q}=0$, we optimized, for the germanide as well as for the silicide, the canting angle assuming ferromagnetic coupling between successive planes along the c axis by keeping the experimental in-plane AFM coupling. The optimized canting angle θ_0 is 65° for $LaMn_2Ge_2$ and $\theta_0=53°$ for $LaMn_2Si_2$ (see Figs. 4 and 5). The calculated total magnetic moments per Mn atom at the optimized canting angles are $3.00\mu_B$ for $LaMn_2Ge_2$ and $2.57\mu_B$ for $LaMn_2Si_2$, both in fairly good agreement with experiments.[12] Although the optimized canting angles differ from the experimental ones (58° and 25° for germanide and silicide, respectively), the tendency towards an increasing canting when replacing Ge for Si is well reproduced in the present calculations.

TABLE I. Calculated and experimental equilibrium in-plane lattice parameter, a_0, and corresponding local Mn magnetic moments for different calculated magnetic structures of $LaMn_2Ge_2$. (1) Ferromagnetic (FM) structure (FM coupling in and between planes) corresponding to $q_z=0$ and $\theta=90°$. (2) Antiferromagnetic 1 (AFM1) structure (AFM coupling in and between planes) corresponding to $q_z=2\pi/c$ and $\theta=90°$. (3) Spiral spin-density-wave (SSDW) structure calculated at the experimental $q_z=0.71(2\pi/c)$ and $\theta=58°$. The LDA showed that the SSDW structure is the ground state in good agreement with experiment, while surprisingly the GGA showed incorrectly that the AFM1 is the ground state. The values of a_0 and μ_{Mn} for those LDA and GGA ground states as well as the experimental values are displayed in bold.

$LaMn_2Ge_2$	a_0 (a.u.)			$\mu_{Mn}(\mu_B)$		
	FM	AFM1	SSDW	FM	AFM1	SSDW
LDA	7.57	7.65	**7.62**	1.93	2.62	**2.47**
GGA	7.76	**7.89**	7.88	2.20	**3.14**	3.07
Experimental			**7.92**			**3.06**

In Table II, we compare these results with the energies obtained for different collinear arrangements. Besides the FM and AFM1 configurations, we also considered other collinear cases, namely, the AFM2 configuration, exhibiting an in-plane AFM coupling and a FM coupling between the (001) planes, as well as the AFM3 configuration, consisting of an in-plane FM coupling and an AFM coupling between the (001) planes. For $LaMn_2Si_2$, the optimized canted magnetic arrangement lies lower in energy than any other considered collinear structure. In the case of $LaMn_2Ge_2$, the optimized canted structure lies higher in energy than the collinear AFM2 structure. In Figs. 4 and 5, it is clearly shown that the value of the magnetic moment of Mn also depends on the canting angle. Together with its dependence on the Mn-Mn interatomic distance and on the neighboring atom type (Si or Ge), this complex behavior of the magnetic moment is another manifestation of the richness of the magnetic interactions in systems containing Mn.

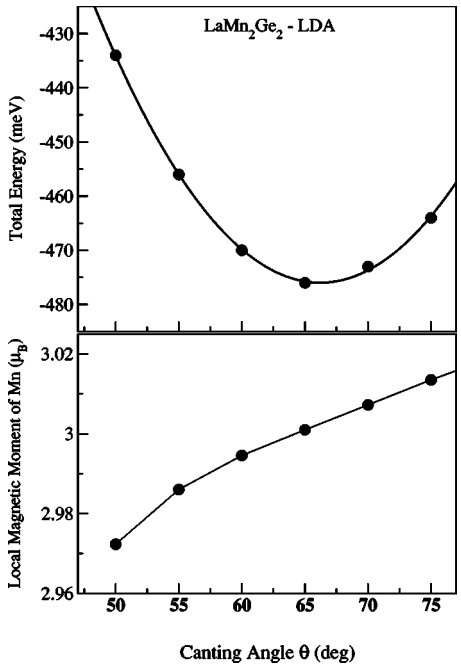

FIG. 4. Total energy per unit cell of $LaMn_2Ge_2$ calculated within the LDA as a function of the canting angle for the experimental volume and $q_z=0$. The energies are given with respect to the FM configuration at the experimental volume.

2. Spin spirals in $LaMn_2Ge_2$ *and* $LaMn_2Si_2$

As seen in the last section, for $LaMn_2Ge_2$ a collinear configuration is lower in energy than the canted magnetic structure. Therefore, we introduced spin spirals with **q** vectors along the experimentally observed direction, that is $(0,0,q_z)$, and studied the evolution of total energy as a function of q_z for different canting angles. For this system, SSDWs for three different canting angles, $\theta=58°$, 60°, and 65° were considered. We chose these canting angles because they lie close to the optimized value θ_0 for $q_z=0$. In Fig. 6, this evolution as a function of the spin-spiral angle $\alpha=\pi q_z$ is shown. The lowest energy was found for a canting angle $\theta_0=60°$ and a spin-spiral wave vector of $q_z=0.64\ (2\pi/c)$.

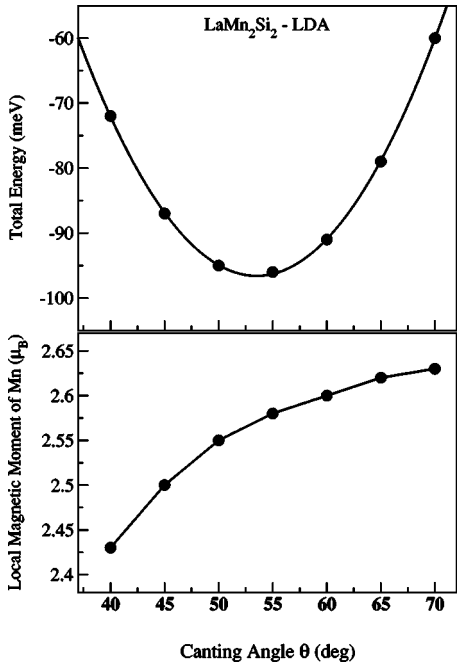

FIG. 5. Same as Fig. 4 but for $LaMn_2Si_2$.

TABLE II. Calculated total energy per unit cell relative to the ferromagnetic (FM) structure and local Mn magnetic moments, μ_{Mn}, for different magnetic structures (all calculations are performed at the experimental in-plane lattice parameter). (1) FM structure [FM coupling in and between the (001) planes] corresponding to $q_z=0$ and $\theta=90°$. (2) AFM1 structure (AFM coupling in and between the planes) corresponding to $q_z=2\pi/c$ and $\theta=90°$. (3) AFM2 structure (in-plane AFM coupling and FM coupling between planes) corresponding to $q_z=0$ and $\theta=90°$. (4) AFM3 structure (in-plane FM coupling and AFM coupling between the planes) corresponding to $q_z=2\pi/c$ and $\theta=90°$. For $q_z=0$ and the turning angle $\alpha=0$, the optimal canting angle θ_0 that minimizes the total energy is $\theta_0=65°$ for $LaMn_2Ge_2$ and $\theta_0=53°$ for $LaMn_2Si_2$, and when α is allowed to vary, the total energy is minimal for $\theta_0=60°$, $\alpha_0=115°$ for $LaMn_2Ge_2$ and $\theta_0=53.5°$, $\alpha_0=135°$ for $LaMn_2Si_2$. The results for these structures are shown in the last two lines of the table. Notice that the value of q_z depends only on whether the coupling between planes is FM or AFM and that both q_z and θ are independent of the nature of the in-plane coupling.

	$LaMn_2Ge_2$		$LaMn_2Si_2$	
Configuration	Energy (eV)	μ_{Mn} (μ_B)	Energy (eV)	μ_{Mn} (μ_B)
FM	0.000	2.33	0.000	2.03
AFM1	−0.441	3.04	0.002	2.69
AFM2	−0.479	3.03	0.001	2.67
AFM3	−0.075	2.33	−0.055	2.08
$\theta_0, \alpha=0$	−0.476	3.00	−0.096	2.57
θ_0, α_0	−0.520	3.00	−0.179	2.62

The corresponding energy is 41 meV lower than for the AFM2 structure and is energetically favored over the other two collinear configurations. This result is in good agreement with what we obtained above for $\mathbf{q}=0$ and is surprisingly close to the experimental value ($\theta_{exp}=58°$). When the SSDW is introduced, the canting angle θ_0 that minimizes the total energy shifts towards a lower value, closer to the experimental one. The optimum value of q_z, 0.64 ($2\pi/c$), is in very good agreement with the experimental one, 0.71 in the same units, at 2 K. The magnetic configuration for which the z component of the Mn moment vanishes, i.e., the flat in-plane spiral, is energetically disfavored at 0 K. At the experimental volume, the difference in the total energy between conical structures and flat spirals is around 52 meV, corresponding to 600 K. Experimentally, a transition from the conical to an in-plane helical structure occurs at 322 K. Considering that thermal fluctuations will bring the transition temperature to a lower value than what can be expected from total-energy calculations at $T=0$ K, the obtained energy differences give already a rough estimate of the behavior of the magnetic order at higher temperatures.

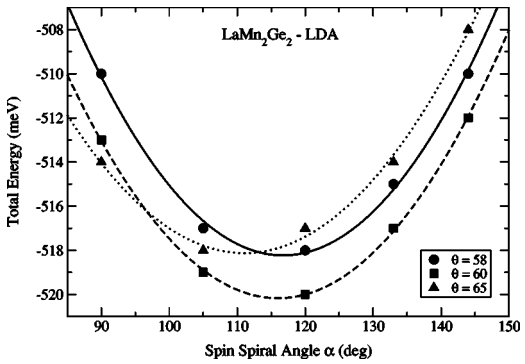

FIG. 6. LDA total energy per unit cell of $LaMn_2Ge_2$ at the experimental volume as a function of the spin spiral angle $\alpha=\pi q_z$ for three different canting angles θ. The energies are given with respect to the FM configuration at the experimental volume.

In the case of $LaMn_2Si_2$, we did a similar study of the total energy as a function of q_z, now for three canting angles $\theta=50°$, 52°, and 55°. We chose these values taking into account that without SSDWs, the magnetic arrangement with minimum energy is given by $\theta_0=53°$ and that the optimum canting angle does not change appreciably when introducing the SSDWs. It can be seen from Fig. 7 that, as expected, the SSDWs lower the energy of the canted structures. Experimentally, this system evolves as a function of temperature from a conical SSDW to a canted arrangement (below 50 K), and at higher temperatures (around 315 K) it changes into the AFM1 structure. The optimized q_z value obtained for $LaMn_2Si_2$ is 0.75 $2\pi/c$ and the canting angle is $\theta=53.5°$. To determine this last value, we calculated the total energy of an extra magnetic configuration, $\theta=60°$, $\alpha=130°$, and performed a quadratic interpolation, as is shown in the inset of Fig. 7. The experimental values are 0.91 $2\pi/c$ and 25°, re-

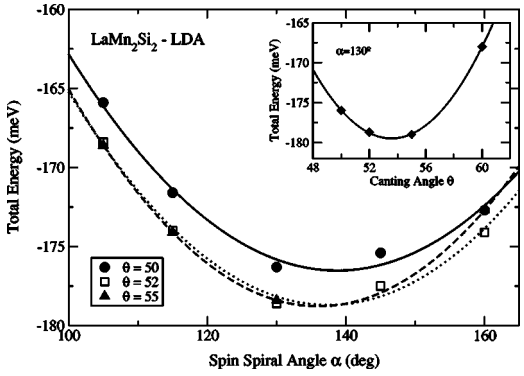

FIG. 7. Same as Fig. 6 but for $LaMn_2Si_2$. In the inset, details of the quadratic fitting done for $\alpha=130°$ are shown.

TABLE III. Comparison between calculated and experimental Mn equilibrium magnetic moments μ_{Mn}, θ_0, and q_z. Calculations are done at the experimental lattice parameters.

		μ_{Mn} (μ_B)	θ_0 (°)	$q_z(2\pi/c)$
$LaMn_2Ge_2$	Calculated	3.00	60.0	0.64
	Experimental	3.06	58.0	0.71
$LaMn_2Si_2$	Calculated	2.62	53.5	0.75
	Experimental	2.43	25.0	0.91

spectively. Even if the agreement with experiments is less favorable than in the case of $LaMn_2Ge_2$, here the trends are also obtained, i.e., the equilibrium canting angle for the silicide is smaller than for the germanide, while the q_z value is larger. The larger differences between experimental and calculated q_z and θ values for the system containing Si, with respect to the differences obtained for Ge, can be traced back to the local moments of Mn, μ_{Mn}, calculated at the experimental volumes, whose theoretical value reproduces well the experimental one for $LaMn_2Ge_2$ while it is 7.8% larger for the Si system. Considering that the relevant energy differences between different collinear structures are about 50 meV, the relevant energy scale for the proper determination of cone angles lies around 10 meV, and that for the determination of spin-spiral wave vectors it is about 2 meV, one understands that a small change of the magnetic moment could lead to significant energy changes. Actually, given a canting angle, the magnetic moments do not depend strongly on the q_z value of the SSDW. Even if thermal fluctuations are certainly going to influence the evolution of the magnetic structure of $LaMn_2Si_2$ with temperature, from Fig. 7 and Table II it can be seen that starting from the conical SSDW configuration at very low temperatures, $LaMn_2Si_2$ evolves to a canted magnetic structure, and from there, at higher tem-

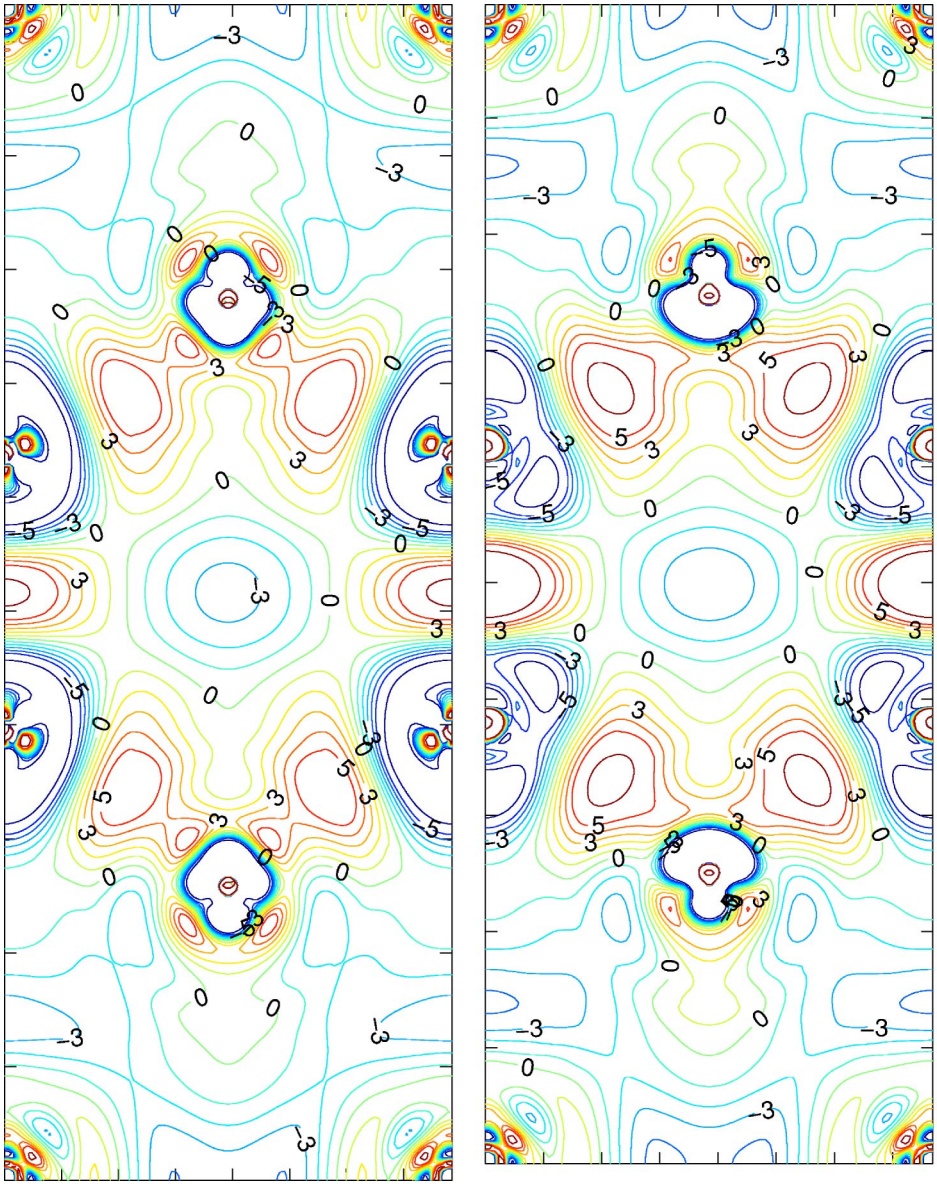

FIG. 8. (Color online) Charge-density difference contours (in electrons $\times 10^{-3}$/a.u.^{3}) for (a) $LaMn_2Ge_2$ and (b) $LaMn_2Si_2$ in the (100) plane.

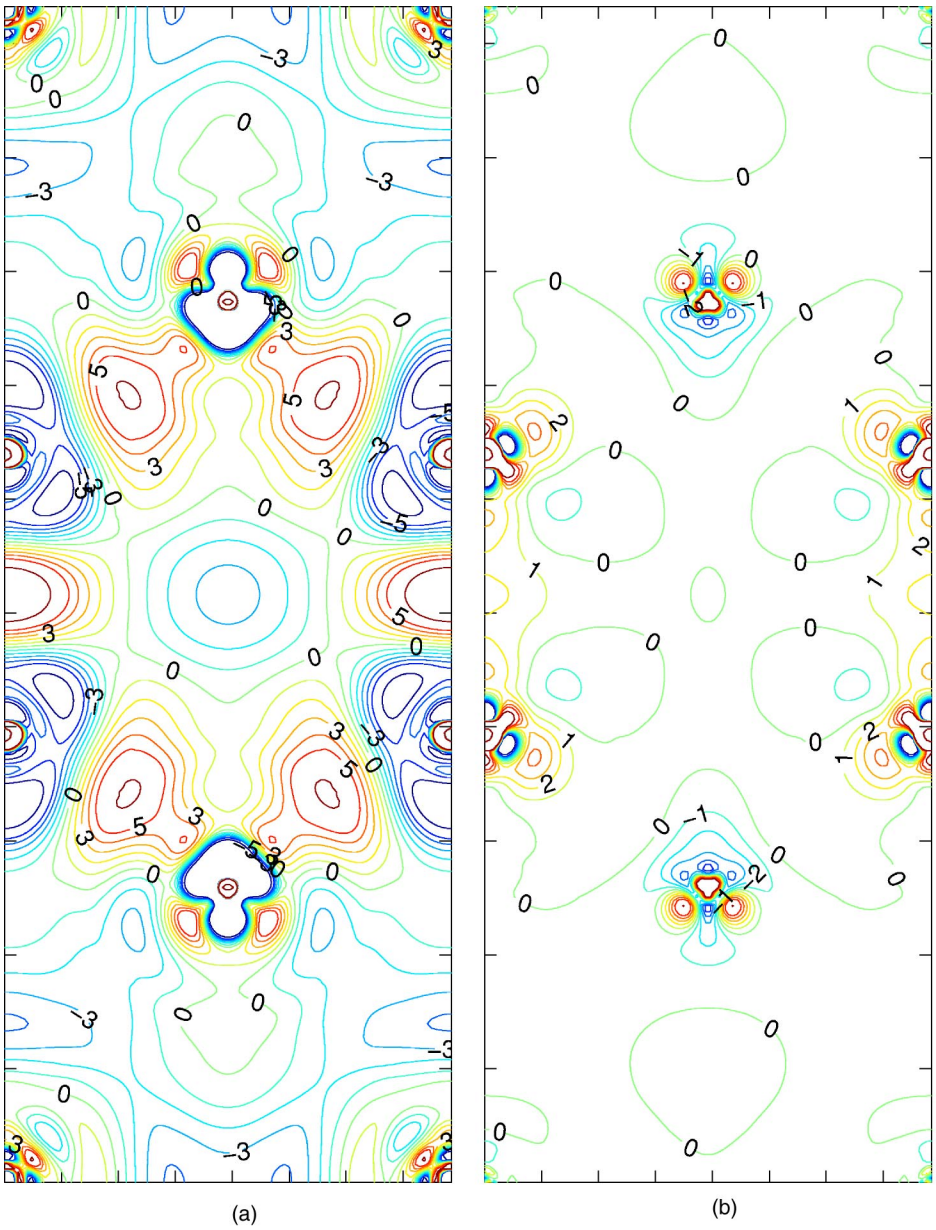

FIG. 9. (Color online) (a) Charge density difference contour plots (in electrons $\times 10^{-3}$/a.u.^{3}) of $LaMn_2Si_2$ in the $LaMn_2Ge_2$'s structure in the (100) plane. (b) Difference between $LaMn_2Si_2$ in $LaMn_2Ge_2$'s structure [Fig. 9(a)] and $LaMn_2Ge_2$ [Fig. 8(a)].

peratures, to a collinear one. This is exactly what happens experimentally. In the case of $LaMn_2Ge_2$, the situation is not as clear as the energy differences are smaller. A summary of the results presented in this subsection is shown in Table III.

C. Dependence of Mn's magnetic moments on Mn-Mn intralayer distances and the role of hybridization

We have seen that Mn's magnetic moment and magnetic interactions depend on Mn-Mn distances. It is interesting to find out whether the differences observed between the magnetic moments of $LaMn_2Ge_2$ and $LaMn_2Si_2$ are only related to their different Mn-Mn distances or if the different hybridization strengths of these systems do play some role. For this purpose, we replaced Ge by Si but kept the lattice parameters of the system fixed at the experimental values of the germanide. For this system, we calculated the FM structure and obtained a Mn magnetic moment of $2.29\mu_B$, while in the $LaMn_2Si_2$ volume it is $2.03\mu_B$. The magnetic moment of Mn in $LaMn_2Ge_2$ is $2.33\mu_B$. We see that μ_{Mn} depends, as expected, primarily on the Mn-Mn distances, but that a hybridization effect is also present.

In Figs. 8 and 9, we show charge-density plots in the (100) plane, from which the corresponding superposition of atomic charge densities has been subtracted, so that the degree of bonding between the constituent atoms can be observed. Higher values of the difference change densities mean stronger bonding. La atoms are located at the corners. In Fig. 9(b), the difference between the bondings in the germanide and in the silicide with the germanide lattice parameters is also shown. From these plots it is straightforward to see that the $LaMn_2Si_2$ system in its own structure shows the largest *X*-Mn hybridization. However, it is surprising that $LaMn_2Si_2$ exhibits even in the structure of $LaMn_2Ge_2$ a larger *X*-Mn hybridization than $LaMn_2Ge_2$. It is due to this

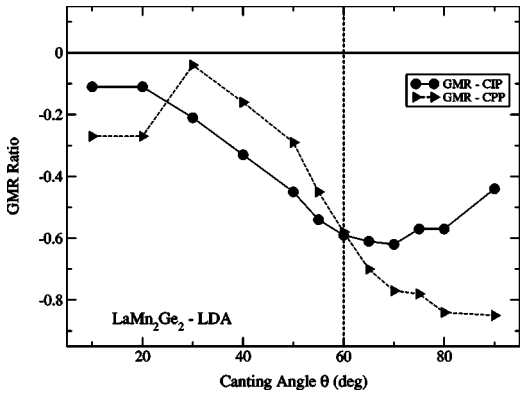

FIG. 10. GMR ratios as a function of the canting angle θ for $LaMn_2Ge_2$. The vertical dashed line indicates the optimum canting angle with SSDW included.

extra hybridization in the case of $LaMn_2Si_2$ that μ_{Mn} is smaller than expected.

D. Transport properties of $LaMn_2Ge_2$

$LaMn_2Ge_2$ has been reported to have an inverse magnetoresistance at low temperatures.[13] In the presence of a magnetic field of 70 kOe, the value of the magnetoresistance increases to an unusually large value at 4.2 K. The large absolute value of the GMR obtained is typical for artificial multilayers, which generally show direct GMR coefficients. The origin of this inverse GMR is, so far, not understood. In a previous work, we calculated the band contribution to the GMR within the semiclassical Boltzmann approximation performing a fixed-spin-moment calculation, that is, constraining the average magnetic moment per Mn atom to be equal to the experimental value.[28] For the average canted configuration, we obtained a small inverse CPP-GMR in the *z* direction. We present here the results obtained when noncollinearity is explicitly taken into account in the electronic structure calculations. In Fig. 10, we show the evolution of the band contribution to the GMR as defined in Eq. (3) as a function of the canting angle θ, for systems with $q_z=0$, considering that the relaxation time for the FM and for the non-FM configurations is the same. We find that the band contribution to the GMR is always direct, in opposition to the experimental observation of an inverse GMR. Thus, the experimental behavior cannot be attributed to the bands. Applying an external magnetic field **H** in the *z* direction, the canting angle decreases with increasing **H**. Since the difference in energy between the conical SSDW and the FM structures at the experimental volume is very large, around 500 meV (Fig. 3), extremely large magnetic fields would be needed to align the magnetic moments of this system. This is exactly what is being observed in the experiments,[13] as the value of the GMR does not saturate even at 70 kOe. The applied field can induce spin fluctuations of lower energy, which should give rise to scattering effects and thereafter to growing resistivities. These scattering effects should go into the relaxation times τ in Eq. (2), which might become smaller with increasing alignment of the magnetic moments (increasing value of **H**). This mechanism had already been suggested by Mallik[13] as one of the possible explanations for the observed behaviors. Even if for the silicides the energy difference between the FM state and the conical SSDW is smaller than for the germanides, it is still sufficiently large to be able to excite lower-energy SSDW's. Also in this case, the GMR is expected to be inverse and increasing with increasing field.

IV. CONCLUSIONS

In this contribution, we have undertaken a systematic study for two systems belonging to the family of intermetallic compounds RMn_2X_2, which exhibit a rich variety of magnetic behaviors, typical of systems containing rare earth atoms and manganese. The calculations are performed by means of the FLEUR code within the LDA and the GGA approximations to the DFT for the exchange-correlation potential. We have selected two systems, $LaMn_2Ge_2$ and $LaMn_2Si_2$, in which the interplay and competition of different interactions give rise to conical helical magnetic arrangements of the magnetic moments of the Mn atoms at low temperatures.

Our first-principles total energy calculations show that the GGA overestimates the stability of the collinear antiferromagnetic structure and fails to reproduce the correct magnetic ground state. The LDA fails to reproduce the proper equilibrium lattice constants by 4%. We speculate that the on-site correlation of Mn is underestimated by both approximations. However, performing the calculations within the LDA approximation at the experimental lattice parameters, the experimental trends shown by these systems are well reproduced and the correct magnetic ground states are obtained for both systems.

We have shown that not only are Mn-Mn distances important for the determination of the ground-state magnetic configuration, but that also the hybridization between Mn and Si or Ge plays an important role. We found that the smaller lattice constant of the silicide leads to a stronger Mn-Mn hybridization, resulting in a smaller local Mn moment and stronger dependencies of the magnetic moment and the total energy on the cone angle, when compared to the germanide.

We have also shown that the GMR of these systems is highly dependent on the canting angle, but that the band contribution by itself cannot explain the large inverse GMR values which grow with the applied magnetic field and which are still not saturated for $H=70$ kOe. We argue that this growing inverse GMR has its origin in the large amount of noncollinear configurations with energies close to the ground state, which can be easily excited with the applied fields and which should give rise to a growing magnetic disorder. The fact that the difference in energy between SSDW configurations and collinear ones is very large is the reason why the GMR does not saturate in the experiments,[13] as the FM case is never reached with the applied magnetic fields.

ACKNOWLEDGMENTS

This work was partially funded by UBACyT-X115, the European Research Training Network (RTN) (Contract

No. HPRN-CT-2000-00143), the French-Argentinian collaboration program ECOS-SETCIP A00E04, and the German-Argentinian collaboration program DAAD-Fundación Antorchas. A.M.L. belongs to Consejo Nacional de Investigaciones Científicas y Técnicas CONICET (Argentina).

*Present address: Departamento de Física, Comisión Nacional de Energía Atómica, Avenida del Libertador 8250, 1429 Buenos Aires, Argentina.

[1] J. Enkovaara, A. Ayuela, J. Jalkanen, L. Nordström, and R. M. Nieminen, Phys. Rev. B **67**, 054417 (2003).
[2] K. Nakamura, T. Ito, A. J. Freeman, L. Zhong, and J. Fernandez-de-Castro, Phys. Rev. B **67**, 014405 (2003).
[3] D. Hobbs, J. Hafner, and D. Spišak, Phys. Rev. B **68**, 014407 (2003).
[4] J. Hafner and D. Hobbs, Phys. Rev. B **68**, 014408 (2003).
[5] L. M. Sandratskii and G. H. Lander, Phys. Rev. B **63**, 134436 (2001).
[6] L. M. Sandratskii and J. Kübler, J. Phys.: Condens. Matter **4**, 6927 (1992).
[7] Ph. Kurz, G. Bihlmayer, K. Hirai, and S. Blügel, Phys. Rev. Lett. **86**, 1106 (2001).
[8] E. Sjöstedt and L. Nordström, Phys. Rev. B **66**, 014447 (2002), and references therin.
[9] B. Malaman, G. Venturini, R. Welter, and E. Ressouche, J. Alloys Compd. **210**, 209 (1994).
[10] G. Venturini, B. Malaman, and E.Ressouche, J. Alloys Compd. **241**, 135 (1996).
[11] M. Hofmann, S. J. Campbell, S. J. Kennedy, and X. L. Zhao, J. Magn. Magn. Mater. **176**, 279 (1997).
[12] G. Venturini, R. Welter, E. Ressouche, and B. Malaman, J. Alloys Compd. **210**, 213 (1994).
[13] R. Mallik, E. V. Sampathkumaran, and P. L. Paulose, Appl. Phys. Lett. **71**, 2385 (1997).
[14] J. M. George, L. G. Pereira, A. Barthélémy, F. Petroff, L. Steren, J. L.Duvail, and A. Fert, Phys. Rev. Lett. **72**, 408 (1994).
[15] Ph. Kurz, F. Förster, L. Nordström, G. Bihlmayer, and S. Blügel, Phys. Rev. B **69**, 024415 (2004).
[16] E. Wimmer, H. Krakauer, M. Weinert, and A. J. Freeman, Phys. Rev. B **24**, 864 (1981); M.Weinert, E. Wimmer, and A. J. Freeman, *ibid.* **26**, 4571 (1982).
[17] L. M. Sandratskii, Adv. Phys. **47**, 91 (1998).
[18] D. M. Bylander and L. Kleinman, Phys. Rev. B **59**, 6278 (1999).
[19] M. I. Katsnelson and V. P. Antropov, Phys. Rev. B **67**, 140406(R) (2003).
[20] V. L. Moruzzi, J. F. Janak, and A. R. Williams, *Calculated Electronic Properties of Metals* (Pergamon, New York, 1978).
[21] P. Perdew andY. Wang, in *Electronic Structure of Solids*, edited by P. Zieshe and H. Eschrig (Akademie Verlag, Berlin, 1991), p. 11.
[22] J. P. Perdew, K. Burke, and M.Ernzerhof, Phys. Rev. Lett. **77**, 3865 (1996).
[23] C. Herring, in *Magnetism*, edited by G. Rado and H. Suhl (Academic Press, New York, 1966), Vol. 4.
[24] J. Ziman, *Electrons and Phonons* (Oxford University Press, London, 1960).
[25] O. Jepsen and O. K. Andersen, Solid State Commun. **9**, 1763 (1971); G. Lehmann and M. Taut, Phys. Status Solidi B **54**, 469 (1972).
[26] G. Venturini, J. Alloys Compd. **232**, 133 (1996).
[27] D. J. Singh and J. Ashkenazi, Phys. Rev. B **46**, 11 570 (1992).
[28] J. Milano and A. M. Llois, Phys. Status Solidi B **220**, 409 (2000).